J Neurophysiol 98: 3473–3485, 2007.
First published September 26, 2007; doi:10.1152/jn.00342.2007.

Concurrent Encoding of Frequency and Amplitude Modulation in Human Auditory Cortex: Encoding Transition

Huan Luo,[1,2,5] Yadong Wang,[1,2,4] David Poeppel,[1,2,4] and Jonathan Z. Simon[1,2,3]

[1]*Neuroscience and Cognitive Science Program and* [2]*Departments of Biology,* [3]*Electrical and Computer Engineering, and* [4]*Linguistics, University of Maryland, College Park, Maryland; and* [5]*State Key Laboratory of Brain and Cognitive Science, Institute of Biophysics, Chinese Academy of Sciences, Beijing, China*

Submitted 27 March 2007; accepted in final form 23 September 2007

Luo H, Wang Y, Poeppel D, Simon JZ. Concurrent encoding of frequency and amplitude modulation in human auditory cortex: encoding transition. *J Neurophysiol* 98: 3473–3485, 2007. First published September 26, 2007; doi:10.1152/jn.00342.2007. Complex natural sounds (e.g., animal vocalizations or speech) can be characterized by specific spectrotemporal patterns the components of which change in both frequency (FM) and amplitude (AM). The neural coding of AM and FM has been widely studied in humans and animals but typically with either pure AM or pure FM stimuli. The neural mechanisms employed to perceptually unify AM and FM acoustic features remain unclear. Using stimuli with simultaneous sinusoidal AM (at rate f_{AM} = 37 Hz) and FM (with varying rates f_{FM}), magnetoencephalography (MEG) is used to investigate the elicited auditory steady-state response (aSSR) at relevant frequencies (f_{AM}, f_{FM}, $f_{AM} + f_{FM}$). Previous work demonstrated that for sounds with slower FM dynamics ($f_{FM} < 5$ Hz), the phase of the aSSR at f_{AM} tracked the FM; in other words, AM and FM features were co-tracked and co-represented by "phase modulation" encoding. This study explores the neural coding mechanism for stimuli with faster FM dynamics ($\leq$30 Hz), demonstrating that at faster rates ($f_{FM} > 5$ Hz), there is a transition from pure phase modulation encoding to a single-upper-sideband (SSB) response (at frequency $f_{AM} + f_{FM}$) pattern. We propose that this unexpected SSB response can be explained by the additional involvement of subsidiary AM encoding responses simultaneously to, and in quadrature with, the ongoing phase modulation. These results, using MEG to reveal a possible neural encoding of specific acoustic properties, demonstrate more generally that physiological tests of encoding hypotheses can be performed noninvasively on human subjects, complementing invasive, single-unit recordings in animals.

INTRODUCTION

A fundamental issue in auditory neuroscience concerns the nature of the computation that transforms the sensory signal into a representation that is useful for auditory tasks (Smith and Lewicki 2006). Complex sounds, especially natural sounds, can be parametrically characterized by many acoustic and perceptual features, one among which is temporal modulation. Temporal modulations describe changes of a sound in amplitude (AM) or in frequency (FM). AM and FM are fundamental components of communication sounds, such as human speech and species-specific vocalizations, as well as music. In human psychophysical experiments with speech stimuli, low-frequency AM features were found to be crucial for speech identification and recognition (Drullman et al. 1994; Shannon et al. 1995), and FM cues were additionally shown to be important in speech recognition, particularly in noise (Zeng et al. 2005). Furthermore, these temporal modulation features are known to be encoded in the auditory system. Numerous neurophysiological studies in animals have indicated that precise timing information is preserved throughout the ascending auditory pathways (Eggermont and Ponton 2002; Elhilali et al. 2004; Heil 1997; Oertel 1997, 1999; Philips et al. 2002; Rose and Metherate 2005). Using reverse correlation techniques, it can be shown that the response properties of auditory cortical neurons are dominated by transient changes in both amplitude and frequency, reflecting their selectivity for AM and FM features in the stimulus sounds (deCharms et al. 1998; Depireux et al. 2001; Elhilali et al. 2004; Miller et al. 2002). Interestingly, the reverse approach, which makes the theoretical assumption that the auditory system's encoding mechanisms are shaped to represent natural sounds in the most optimal and efficient way, predicts a preponderance of AM and FM response patterns in the receptive fields of auditory cortical neurons (Klein et al. 2003; Lewicki 2002).

Magnetoencephalography (MEG), a noninvasive brain imaging technique, provides a macroscopic measure of spatiotemporal patterns of underlying neural ensemble activities at high temporal resolution ($\sim$1 ms), making it a suitable and efficient tool to track the processing of temporal modulation features in the human brain. The recorded MEG signals represent the neural population responses or system activities, which have long been suggested to play significant roles in encoding mechanisms (Nicolelis et al. 1997; Wilson and McNaughton 1993) but are difficult to access from traditional microscopic-level neurophysiological studies. Under the appropriate experimental circumstances, MEG data may provide an excellent link between macroscopic neural activity and the encoding mechanisms principally developed based on single-unit data.

It has been consistently demonstrated in animal neurophysiological studies that slow AM and FM rates are explicitly represented in the auditory cortex by temporal coding, since neurons fire phase-locked spikes in response to amplitude or frequency changes in the stimulus (e.g., Eggermont 1994; Liang et al. 2002; Schreiner and Urbas 1986; Wang et al. 2003). At faster stimulus modulation rates, rate coding (overall spike rate) instead of temporal coding (timed spike discharge) may be seen (Lu et al. 2001). Neuroimaging techniques have

Address for reprint requests and other correspondence: H. Luo, State Key Laboratory of Brain and Cognitive Science, Institute of Biophysics, Chinese Academy of Science, 15 Datun Rd., Beijing 100101, China (E-mail: luohuan@gmail.com).

The costs of publication of this article were defrayed in part by the payment of page charges. The article must therefore be hereby marked "*advertisement*" in accordance with 18 U.S.C. Section 1734 solely to indicate this fact.

also been extensively used as a tool to study the processing and representation of temporal modulation features in human auditory cortex. Functional magnetic resonance imaging (fMRI) and intracortical recording experiments have revealed sustained cortical responses to AM and FM sound stimuli that vary in magnitude and shape as the stimulus modulation rates increase >10 Hz (Giraud et al. 2000; Harms and Melcher 2002; Haller et al. 2005; Hart et al. 2003; Langers et al. 2003; Liegeois-Chauvel et al. 2004). Ahissar et al. (2001) found that one component of the MEG signal correlated well with the slow temporal envelope of its speech stimulus and was able to predict its intelligibility. In most MEG and electroencephalographic (EEG) experiments on humans using AM or FM stimuli, the auditory steady-state response (aSSR), an elicited response with the same frequency of the corresponding stimulus modulation frequency, is the main approach to examining AM and FM representations. aSSRs have been found for stimulus modulation rates ≤200 Hz (Picton et al. 2003; Ross et al. 2000, 2005).

AM and FM have been widely studied in both animals and humans, where the auditory system is typically probed with *either* AM or FM stimuli. However, most natural communication sounds (e.g., human speech, marmoset calls, bird songs, etc.) contain simultaneous temporal modulations in both amplitude and frequency. In fact it is a standard mathematical result that any band-passed signal can be described in its entirety as simultaneous but separate AM and FM components (Papoulis 1962). In other words, AM and FM always co-occur and are inseparable acoustic features of an auditory object, and therefore the auditory system should be able to co-track them to achieve "perceptual unity" of the incoming sound. Note that co-tracking refers to a combinational encoding of AM and FM features, and it differs from simultaneous tracking, in which the resultant neuronal activity is simply a sum of the two separate tracking signals for AM and FM, respectively (see, e.g., Cariani 2004) (see also discussion on feature grouping in the following text). There have been at least two examples of such co-tracking found in auditory systems. In an experiment on ferrets using spectrotemporally complex sounds containing simultaneous AM and FM, cortical neurons (which are sensitive only to bandpassed versions of the original signal, due to cochlear processing) demonstrated the ability to fire spikes phase-locked to both slow-rate AM and fast-rate FM (Elhilali et al. 2004). In a study on human auditory processing, Patel and Balaban (2003) found that the phase of the MEG aSSR at the envelope modulation frequency could dynamically track tone-sequence stimuli, suggesting a relationship between AM and FM processing in auditory cortex and a possible co-tracking mechanism.

We employ acoustic stimuli sinusoidally modulated in both amplitude (AM, at rate f_{AM}) and frequency (FM, at rate f_{FM}). These stimuli are a simplification of natural sounds containing simultaneous AM and FM, but their dynamics can be described simply by the two frequency parameters f_{AM} and f_{FM}. In turn, we can examine their representations in the human brain by measuring the spectra of the neural MEG responses at frequencies related to these stimulus parameters. In addition, by varying these parameters, we can investigate coding transitions as a function of stimulus rate dynamics, perhaps analogous to the temporal-to-rate coding transition observed in click studies in marmoset auditory cortex (Lu et al. 2001).

In previous work (Luo et al. 2006), for stimuli with slow FM ($f_{FM} < 5$ Hz), we observed in the MEG signal spectral components at the AM frequency and two sidebands at $f_{AM} - f_{FM}$, f_{AM}, $f_{AM} + f_{FM}$. This spotlights "modulation encoding" and, in particular, phase modulation (PM) as a way to co-represent AM and FM simultaneously. Modulation is a widely used encoding scheme in both nature and electrical engineering. The most well-known engineering example is radio, in which the target signal (e.g., speech or music) is imposed on the radio station carrier signal by modulating the amplitude or frequency of the electromagnetic carrier signal, corresponding to AM radio or FM radio. There are a wide variety of other modulation encoding methods used for other radio transmission applications, including single sideband, single sideband with suppressed carrier, and double sideband with suppressed carrier. These encoding schemes have the advantage of efficiently transmitting signals even in the presence of noise. Modulation signals have a distinctive signature in their spectrum—the presence of one or two sidebands, with or without carrier, and different modulation-type signals (e.g., AM, FM, and PM signals) can be distinguished based on the phase relationships among those sidebands and the carrier. The same work confirmed PM encoding in the recorded MEG signals for stimuli with slow FM ($f_{FM} < 5$ Hz). Specifically, the neural SSR at the higher AM frequency f_{AM} provides a neural carrier that is modulated in its phase (PM) at the rate of the slower frequency f_{FM}.

In the current experiment, we employ stimuli with faster FM dynamics (f_{FM} 2.1–30 Hz) and investigate the possibility of forms of modulation encoding, for rates faster than ~5 Hz, different from the previously observed PM encoding based on the failure of PM encoding at the highest rates employed in the earlier study. We find a transition from PM encoding to single sideband (SSB) encoding. The SSB response contains only the upper sideband at $f_{AM} + f_{FM}$, and the neural carrier at f_{AM} (i.e., the original SSR induced by the stimulus AM), but is missing the lower sideband at $f_{AM} - f_{FM}$. Neural models suggest that the appearance of SSB responses may be explained by the additional involvement of AM encoding. i.e., neurons for whom their neural carrier response at f_{AM} is modulated in its *amplitude* (not phase) at the slower frequency f_{FM}. In particular, a quadrature relationship (phase shift by 90°) between the PM and AM components of the response is necessary.

METHODS

Fast FM experiment

STIMULI. Nine stimuli were created, using custom-written programs in MATLAB (The MathWorks, Natick, MA), with a sampling frequency of 44.1 kHz. The stimuli were sinusoidally frequency modulated tones with modulation frequencies (f_{FM}) of 2.1, 3.1, 5.1, 8.0, 10.3, 15.1, 20.1, 24.3, and 30 Hz and frequency deviation between 220 and 880 Hz. In addition, the entire stimulus amplitude was modulated sinusoidally at a fixed rate of 37 Hz (f_{AM}) with modulation depth 0.8. All stimuli were 10 s in duration and shaped by rising and falling 100-ms cosine squared ramps. Each stimulus was presented 10 times. Figure 1 shows the temporal waveform (*top*), the spectrogram (*middle*), and the spectrum (*bottom*) of two example stimuli, confirming that the stimulus sounds contain both a sinusoidally modulated temporal envelope at f_{AM} (37 Hz) and a sinusoidally modulated

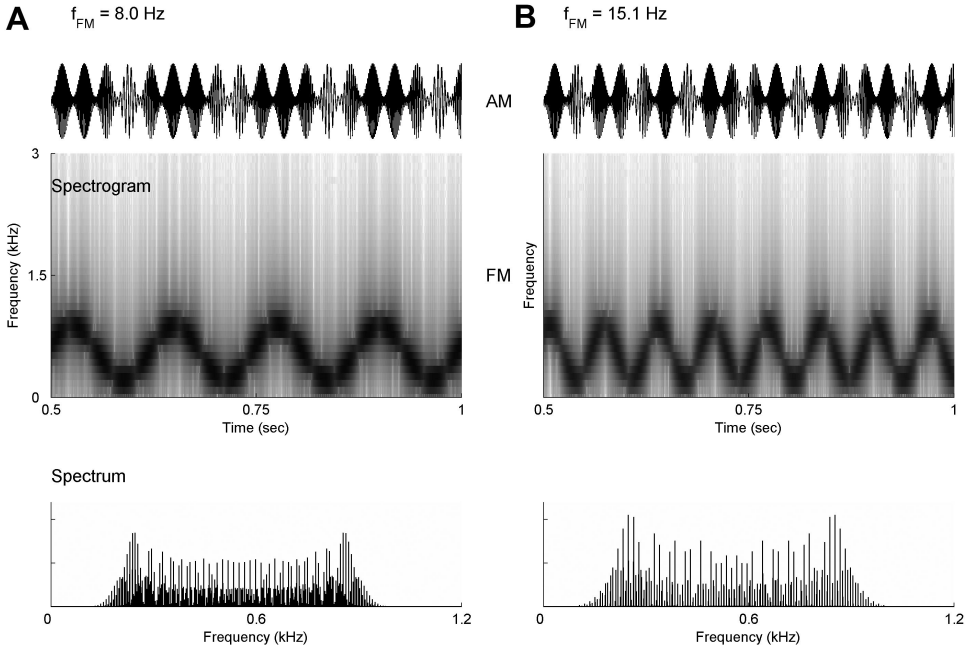

FIG. 1. Stimulus examples with f_{FM} of 8.0 Hz (*A*) and 15.1 Hz (*B*), respectively. *Top*: temporal waveform of stimulus. The temporal envelope was sinusoidally modulated at 37 Hz (f_{AM}). Only 1 segment from 0.5 to 1.0 s is shown to let the modulation be seen more clearly. *Middle*: spectrogram of the same temporal segment (0.5–1.0 s) of the stimulus. Note the carrier frequency is also sinusoidally modulated (*A,* 8.0 Hz; *B,* 15.1 Hz) in the range from 220 to 880 Hz. *Bottom*: spectrum of the stimulus (10-s duration; linear scale). Note that the spectra are broadband.

carrier frequency at f_{FM}. Because the frequency range of the carrier ranges from 220 to 880 Hz, the stimuli have the long-term broadband spectra shown in the *bottom panel.*

To ensure that subjects attended to the long stimulus sequences, 36 distracter stimuli were created and inserted into the experiment for subjects to detect. These distracters were identical to the normal stimuli except that single short-duration FM sweeps were inserted at random times in the stimulus. Subjects were instructed to press a button when they detected the distracter stimuli. Normal stimuli ($90 = 9 \times 10$) and distracter stimuli (36) were mixed and played to subjects in a pseudo-random order at a comfortable loudness level. Subjects performed the required task fairly well (average miss rate: ~4/36; average false alarm rate: ~1/36). The entire experiment was divided into 4 blocks with breaks between each. Data for distracter stimuli were discarded, and only the data for normal stimuli were analyzed.

MEG RECORDINGS. Eleven subjects with normal hearing and no neurological disorders provided informed consent before participating in the experiment. All experimental procedures were approved by the Institutional Review Board (IRB) of the University of Maryland. Before recording began, all subjects were trained to press a button to report the detection of a distracter stimulus. Neuromagnetic signals were collected continuously with a 157-channel whole-head MEG system (5 cm baseline axial gradiometer SQUID-based sensors, KIT, Kanazawa, Japan) in a magnetically shielded room, using a sampling rate of 1000 Hz and an on-line 100-Hz analog low-pass filter, with no high-pass filtering. Each subject's head position was determined via five coils attached to anatomical landmarks (nasion, left and right preauricular points, 2 forehead points) measured at the beginning and the end of recording to ensure that head movement was minimal. Head shape was digitized using a three-dimensional digitizer (Polhemus).

Data analysis

aSSR responses were obtained by calculating the discrete Fourier transform (DFT) of the concatenated responses from 10 trials (100 s = 10 × 10 s) for each of the nine stimulus conditions (varying f_{FM}), giving frequency resolution 0.01 Hz. These calculations were computed for all 157 MEG channels, all nine stimulus conditions, and all 11 subjects. In addition, the phase coefficients were corrected to undo the phase delay introduced by the 60-Hz hardware notch filter. These Fourier coefficients were stored for further analysis for each subject. Examples of the DFT magnitudes are illustrated in Fig. 2.

CHANNEL SELECTION. To increase the signal-to-noise ratio, the 50 (of 157) channels with maximum amplitude at 37 Hz (f_{AM}) were selected per subject. These were regarded as channels representative of auditory cortical activity and used for all further analysis; the remaining channels were not analyzed.

SIDEBAND FREQUENCIES. Target sideband frequencies were defined for different f_{FM} as upper sideband ($f_{AM} + f_{FM}$) and lower sideband ($f_{AM} - f_{FM}$), leading to 18 (9×2) frequencies (upper: 39.1, 40.1, 42.1, 45, 47.3, 52.1, 57.1, 61.3, 67 Hz; lower: 34.9, 33.9, 31.9, 29, 26.7, 21.9, 16.9, 12.7, 7 Hz). The DFT amplitude and phase at every target sideband frequency were extracted for all 50 channels (per subject), and for every stimulus condition, giving a size $89100 = 18 \times 9 \times 50 \times 11$ data set (frequency × stimulus_condition × channel × subject).

SIDEBAND AMPLITUDE MATRIX. We examined the presence of sideband patterns ($f_{AM} \pm f_{FM}$) in the spectra of the MEG signal, a distinctive signature of modulation encoding, by checking whether each specific stimulus condition (characterized by stimulus f_{FM}) induced significant spectral peaks at corresponding sideband frequencies ($f_{AM} \pm f_{FM}$) and not at other sideband frequencies.

For each subject, the amplitudes of a specific sideband frequency were examined for all nine stimulus conditions and for all 50 selected channels, and the results were summed across 50 channels, giving a 9-value vector, which was then normalized by dividing by its mean. This 9-value vector represented the normalized elicited spectral power at this specific sideband frequency under all nine stimulus conditions, so ideally, the maximum value will occur for the entry corresponding to the appropriate stimulus condition. The same procedure was followed for all sideband frequencies (9 upper and 9 lower sideband frequencies separately), giving two 9×9 matrices, corresponding to the upper sideband amplitude matrix (A_{Upper}) and the lower sideband amplitude matrix (A_{Lower}). In each amplitude matrix, the nine rows represent the nine different target sideband frequencies (in A_{Upper}: $f_{AM} + f_{FM}$; in A_{Lower}: $f_{AM} - f_{FM}$), and the nine columns represent the nine different stimulus conditions. Each element in the matrix represents the normalized spectral power at this specific sideband frequency (corresponding row) for a specific stimulus condition (cor-

responding column). Graphical examples of the sideband amplitude matrices can be seen in RESULTS (Fig. 3), illustrating the grand average of these sideband amplitude matrices across subjects.

For directly comparing the sideband amplitudes against each other, we also define an additional pair of amplitude matrices ($A_{\text{Upperdiff}}$, $A_{\text{Lowerdiff}}$). Each element in $A_{\text{Upperdiff}}$ and $A_{\text{Lowerdiff}}$ represents the difference between the absolute amplitude and the background amplitude (mean of its row) at the specific sideband frequency (corresponding row) for a specific stimulus condition (corresponding column). These two new measured parameters are estimates of the fundamental stimulus-elicited signal amplitude (since the measured response reflects the elicited response plus the background response). Use of the background as a reference, whether as a ratio or by subtraction, is necessary due to the wide range sideband frequencies analyzed here (7 Hz, in the theta band, ≤67 Hz, in the gamma band).

ENCODING-TYPE PARAMETER. Both AM and PM encoding elicit a two-sideband spectrum pattern but with different phase relationships between the sidebands and carrier, characterized by the encoding-type parameter α (itself a generalized phase taking on values between 0 and 2π). The encoding-type parameter α is defined as

$$\alpha = (\theta_{\text{upper}} - \theta_{f_{\text{AM}}}) + (\theta_{\text{lower}} - \theta_{f_{\text{AM}}}) \quad (1)$$

where θ is the phase at that frequency, upper $= f_{\text{AM}} + f_{\text{FM}}$, and lower $= f_{\text{AM}} - f_{\text{FM}}$. AM encoding produces α near 0 (or 2π) and PM encoding produces α near π (Luo et al. 2006). α was calculated for all nine sideband frequency pairs under the corresponding stimulus condition, for all 50 selected channels, and for all 11 subjects. Circular statistics (Fisher 1996) were used to estimate the (circular) mean and (circular) SE of α across $n = 550$ samples (50 channels × 11 subjects) for each of the nine sideband frequency pairs.

VECTOR STRENGTH OF α. The vector strength of α (v_α, ranging between 0 and 1) is used to examine the robustness of the encoding-type parameter α. Larger v_α indicates narrower distribution of α, and smaller v_α indicates wider distribution of α; in fact $1 - v_\alpha$ is mathematically equal to the circular variance of the distribution. The vector strength, defined as

$$v_\alpha = \frac{1}{N}\sqrt{\left(\sum_{i=1}^{N}\sin(\alpha_i)\right)^2 + \left(\sum_{i=1}^{N}\cos(\alpha_i)\right)^2} \quad (2)$$

was calculated for all nine sideband frequency pairs and nine stimulus conditions across 550 samples, giving a 9 × 9 matrix V_α. In V_α, the nine rows represent the nine sideband frequency pairs ($f_{\text{AM}} \pm f_{\text{FM}}$) and nine columns represent the nine different stimulus conditions. Each element in the matrix represents the v_α value of this specific sideband frequency pair (corresponding row) for a specific stimulus condition (corresponding column). Ideally, the corresponding stimulus condition should elicit a robustly narrow α distribution and therefore the maximum v_α value in each row. Graphical examples of the vector strength matrix V_α can be seen in RESULTS (Fig. 4).

PHASE DIFFERENCE PARAMETERS. Another two phase parameters, $\theta_{\text{Upperdiff}}$ and $\theta_{\text{Lowerdiff}}$, are used to examine the phase properties of upper and lower sideband frequencies, respectively, complementary to the amplitude properties of sidebands characterized by A_{Upper} and A_{Lower}. They are defined as

$$\begin{aligned}\theta_{\text{Upperdiff}} &= \theta_{\text{Upper}} - \theta_{f_{\text{AM}}}\\ \theta_{\text{Lowerdiff}} &= \theta_{\text{Lower}} - \theta_{f_{\text{AM}}}\end{aligned} \quad (3)$$

Therefore

$$\alpha = (\theta_{\text{Upper}} - \theta_{f_{\text{AM}}}) + (\theta_{\text{Lower}} - \theta_{f_{\text{AM}}}) = \theta_{\text{Upperdiff}} + \theta_{\text{Lowerdiff}} \quad (4)$$

$\theta_{\text{Upperdiff}}$ and $\theta_{\text{Lowerdiff}}$ were calculated for all target sideband frequencies (9 upper sideband frequencies and 9 lower sideband frequencies), all selected 50 channels, all nine stimulus conditions, and all 11 subjects. The same circular statistics used to calculate α were used to estimate the mean ± SE of $\theta_{\text{Upperdiff}}$ and $\theta_{\text{Lowerdiff}}$. Their vector strengths, $v_{\text{Upperdiff}}$ and $v_{\text{Lowerdiff}}$, are defined analogously to the vector strength of α in *Eq. 2*. These calculated vector strength values were used to construct two 9×9 vector strength matrices ($V_{\text{Upperdiff}}$, $V_{\text{Lowerdiff}}$) using the same configuration as that for V_α. In addition, $\theta_{\text{Upperdiff}}$ and $\theta_{\text{Lowerdiff}}$ were then adjusted to compensate for their group delay (latency), as estimated by the slope of the $\theta_{\text{Upperdiff}}$-frequency and $\theta_{\text{Lowerdiff}}$-frequency curves, giving $\theta^{\text{adj}}_{\text{Upperdiff}}$ and $\theta^{\text{adj}}_{\text{Lowerdiff}}$ (which have the same vector strength and SEs as of $\theta_{\text{Upperdiff}}$ and $\theta_{\text{Lowerdiff}}$). Graphical examples of the phase difference vector strength matrix can be seen in RESULTS (Fig. 5).

ASYMMETRY INDEX FOR AMPLITUDE AND VECTOR STRENGTH. The amplitude asymmetry index AI_A and vector strength asymmetry index AI_V quantify any asymmetry between the upper and lower sidebands. They are normalized to lie between −1 and 1 and defined as

$$\begin{aligned}\text{AI}_\text{A} &= \frac{\text{diag}(A_{\text{Upperdiff}} - A_{\text{Lowerdiff}})}{\text{diag}(A_{\text{Upperdiff}} + A_{\text{Lowerdiff}})}\\ \text{AI}_\text{V} &= \frac{\text{diag}(V_{\text{Upperdiff}} - V_{\text{Lowerdiff}})}{\text{diag}(V_{\text{Upperdiff}} + V_{\text{Lowerdiff}})}\end{aligned} \quad (5)$$

Note that AI_A is defined in terms of ($A_{\text{Upperdiff}}$ and $A_{\text{Lowerdiff}}$) rather than (A_{Upper} and A_{Lower}) because the comparisons of the latter pair are confounded by the different signal-to-noise ratios at the upper and lower sideband frequencies. The former pair comparisons are based on the elicited power (power beyond the background power) at the two different frequencies.

SIMULATIONS. We constructed a model neuron population the SSR amplitude and phase of which are both modulated by the stimulus FM. In this model, we posit that the phase modulation index is fixed (at $\pi/8$) (as observed by Ross et al. (2001), but the AM index m may vary with f_{FM}. The goal was to see if an increase in the AM portion of the response, i.e., an increase in m, could account for the observed SSB for high f_{FM} rates

$$S(t) = \underbrace{(1 + m\cos(2\pi f_{\text{FM}}t + \theta))}_{\text{Amplitude Modulation}} \times \underbrace{\cos\left(2\pi f_{\text{AM}}t + \frac{\pi}{8}\cos(2\pi f_{\text{FM}}t)\right)}_{\text{Phase Modulation}} + \text{GWN} \quad (6)$$

As shown in *Eq. 6*, simulated encoding signals $S(t)$ with neural carrier frequency of 37 Hz (f_{AM}) and modulation frequency of 8 Hz (1 example of f_{FM}) were created with additive Gaussian white noise (GWN) at a relative level of 15. The AM index m varies from 0 to 0.8. The parameter θ, characterizing the phase shift of AM contribution to $S(t)$ in relation to the phase modulation contribution of $S(t)$, varies from 0 to 2π. We performed 300 simulations for each AM index parameter m from 0 to 0.8 in step of 0.08 and for each phase shift parameter θ from 0 to 2π in step of $\pi/4$ and calculated parameters ($\theta^{\text{adj}}_{\text{Upperdiff}}$, $\theta^{\text{adj}}_{\text{Lowerdiff}}$, α, AI_A, AI_v) of the simulated signals.

For comparison, we also constructed a model containing a pair of neural populations. The SSR *amplitude* of one population is modulated by the stimulus FM [AM encoding population, $S_{\text{AM}}(t)$], whereas the SSR *phase* of the other population is modulated by the stimulus FM [PM encoding population, $S_{\text{PM}}(t)$].

$$\begin{aligned}S_{\text{PM}}(t) &= \cos\left(2\pi f_{\text{AM}}t + \frac{\pi}{8}\cos(2\pi f_{\text{FM}}t)\right)\\ S_{\text{AM}}(t) &= (1 + 0.25\cos(2\pi f_{\text{FM}}t + \theta))\cos(2\pi f_{\text{AM}}t)\\ S(t) &= \tau S_{\text{AM}}(t) + (1 - \tau)S_{\text{PM}}(t) + \text{GWN}\end{aligned} \quad (7)$$

Both $S_{AM}(t)$ and $S_{PM}(t)$ were created with carrier frequency of 37 Hz (f_{AM}) and modulation frequency of 8 Hz (1 example of f_{FM}). The phase modulation index in $S_{PM}(t)$ and the AM index in $S_{AM}(t)$ are fixed (at $\pi/8$ and 0.25, respectively, as measured by Ross et al. 2001). The simulation mixed signal $S(t)$ were created by combining $S_{AM}(t)$ and $S_{PM}(t)$ using different mixing weights τ (pure PM: $\tau = 0$; pure AM: $\tau = 1$) and then by adding GWN. The parameter θ, also characterizing the phase shift of AM contribution to $S(t)$ in relation to the phase modulation contribution of $S(t)$ varies from 0 to 2π. The relative increase in the AM contribution to the response is given by the mixing weight parameter τ.

Functionally, this paired neural population model is not distinguishable from the previous single neural population model because both of them test for the effect of an increase in the AM contribution of the response. Specifically, in the single neural population model, the AM index parameter m was increased to simulate the increase in the AM contribution to the response; in the paired neural population model, it was the increase of mixing weights τ (pure PM: $\tau = 0$; pure AM: $\tau = 1$) that produced the effect of an increase in the AM contribution. Either could account for the observed SSB for high f_{FM} rates. However, they are different in the hypothesized underlying neuron population structure and encoding properties.

Slow FM experiment

The method used to perform the slow FM experiment has been described earlier (Luo et al. 2006), but the results have been reanalyzed here to complement the analysis of the fast FM experiment paradigm. Nine stimuli were created using the same MATLAB program with f_{AM} of 37 Hz and smaller f_{FM} (0.3, 0.5, 0.8, 1.0, 1.7, 2.1, 3.0, 5.0, 8.0 Hz). Twelve subjects participated in this experiment. The same experiment paradigm and MEG data acquisition condition as that of the fast FM experiment were used.

Instead of the 20 channels/subject selected in the previous analysis, 50 channels with maximum amplitude at 37 Hz (f_{AM}) were selected. The 50 channels always include the 20 channels selected previously. The Fourier coefficients for these selected 50 channels were reanalyzed using the same data analysis methods as described in the preceding text for the slow FM experiment for comparison with results of the fast FM experiment.

RESULTS

Auditory steady-state response

Clear stimulus-evoked aSSR at f_{AM} (37 Hz) was observed for all subjects under all 9 stimulus conditions in both the fast and slow FM experiments because all the stimulus conditions have the same f_{AM} at 37 Hz and only differ in f_{FM}. Figure 2*A* shows the discrete Fourier transform of one channel of a representative subject under nine different stimulus conditions of the fast FM experiment. The spectrum shows a clear peak at 37 Hz (f_{AM}), as indicated by the black arrows. Figure 2*B* shows its corresponding phasor representations (Simon and Wang 2005), and here only stimulus condition 1 ($f_{FM} = 2.1$ Hz) is shown as an example. As in the case for the slow FM experiment (Luo et al. 2006), it indicates a clear bilateral auditory cortical origin of the aSSR at 37 Hz, but claims of localizability beyond that are not warranted.

aSSRs at sideband frequencies were also observed. As illustrated in Fig. 2*A*, each stimulus with different f_{FM} (2.1–30 Hz) elicited corresponding sidebands (here, only upper sidebands are shown), indicated by gray arrows. For example, for stimuli with f_{FM} of 8 Hz, the response spectrum showed a peak at 45 Hz (37 + 8 Hz); for stimuli with f_{FM} of 10.3 Hz, there was a peak at 47.3 Hz (37 + 10.3 Hz); for stimuli with f_{AM} of 15.1 Hz, a spectral peak at 52.1 Hz (37 + 15.1 Hz) was elicited. Note that Fig. 2*A* illustrates the spectrum of the same channel under nine different stimulus conditions, and it clearly indicates that in this case the observed sideband frequency peak was stimulus-elicited.

Direct FM-generated aSSR, i.e., at the frequencies of f_{FM} (2.1–30 Hz), were also observed, in agreement with previous findings (Dimitrijevic et al. 2001; Luo et al. 2006; Picton et al. 1987). For example, the stimulus with f_{FM} of 8 Hz elicited an aSSR response peak at 8 Hz, and the stimulus with f_{FM} of 30 Hz elicited an aSSR response peak at 30 Hz, in addition to any sidebands around the AM generated SSR.

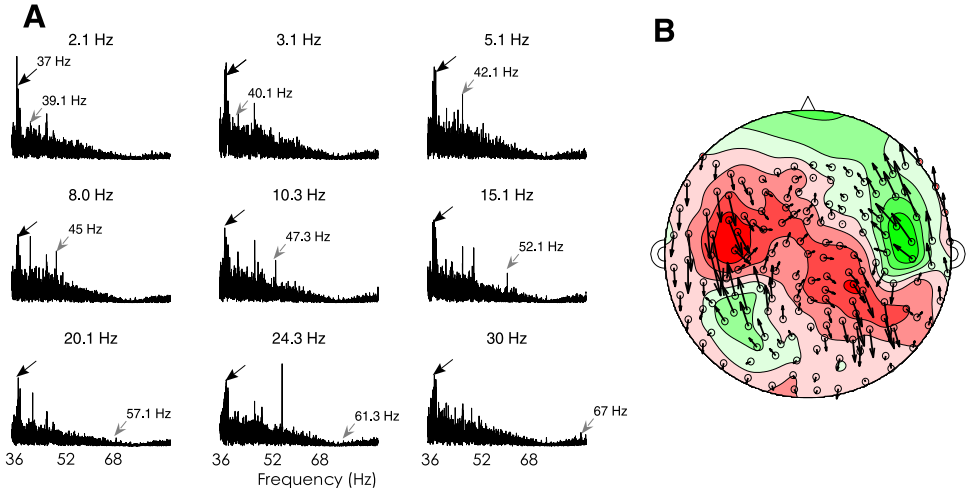

FIG. 2. Auditory steady-state response (aSSR) at f_{AM} (37 Hz) and upper sideband (37 + f_{FM}). *A*: spectrum of the response from 1 representative channel of one subject under all 9 stimulus conditions (different stimulus f_{FM}), denoted by the subtitle value. Black arrows, aSSR at f_{AM} (37 Hz); gray arrows, corresponding upper sideband frequency ($f_{AM} + f_{FM}$) for each specific stimulus condition. For example, the stimulus with f_{FM} of 8.0 Hz (the 1st figure in the 2nd row) elicited aSSR at 45 Hz (37 + 8.0, gray arrow). *B*: phasor representation of aSSR at f_{AM} (37 Hz). It clearly shows a bilateral auditory magnetoencephalographic (MEG) contour map. Arrow length in each channel, aSSR amplitude at 37 Hz; arrow direction, aSSR phase. Note that the channels with largest arrows (largest aSSR at 37 Hz) are centered in the bilateral auditory cortex positions, representing the origin of the elicited aSSR and are the main places where the 50 channels were selected from for further analysis.

Transition from two sidebands to one sideband

As can be seen in Fig. 2*A,* narrow-band system noise coexists with the spectral responses to be detected (f_{AM}, f_{FM}, sidebands), which in turn may make the direct detection of the narrowband response at sideband frequencies more difficult. A method to assess the significance of the narrowband response elicited at a target frequency by the corresponding stimulus, is by an across-condition comparison, shown in the sideband amplitude matrices (A_{Upper}, A_{Lower}).

Figure 3 shows the grand average of the upper (A_{Upper}) and lower (A_{Lower}) sideband amplitude matrices across 11 subjects, and for both the slow FM experiment (Fig. 3, *A* and *D;* f_{FM}: 0.3–8 Hz) and the fast FM experiment (Fig. 3, *B* and *E*; f_{FM}: 2.1–30 Hz). In these matrices, most rows peak on the diagonal, which indicates that those sideband frequencies (rows) were more strongly elicited by the corresponding stimulus (and not by any other stimulus condition). In addition, there are noticeable differences between A_{Upper} (Fig. 3, *A* and *B*) and A_{Lower} (Fig. 3, *D* and *E*). Specifically, A_{Upper} shows a dominant diagonal pattern, whereas this pattern was less expressed in A_{Lower}, especially in the high f_{FM} range (Fig. 3*E*).

Such asymmetrical performance between A_{Upper} and A_{Lower} can be seen more clearly in plots below in Fig. 3, *C* and *F,* illustrating the corresponding nine-value diagonal value vector of A_{Upper} and A_{Lower}, respectively. The slow FM experiment low-f_{FM}-range data (gray line) and the fast FM experiment high-f_{FM}-range data (black line) are plotted in the same figure for comparison. Note that there are four overlapping f_{FM} stimulus conditions (2.1, 3.1, 5.1, 8 Hz) that show consistently good results. The horizontal starred line indicates the mean amplitude level at this frequency, i.e., the noise floor. Specifically, for stimuli with low f_{FM} (<5 Hz), both upper and lower sidebands are strongly elicited [with the exception of 2 outliers in the upper sideband, f_{FM} at 0.3 and 0.5 Hz, which are artificially small due to system narrowband noise at 37.3 and 37.5 Hz (Luo et al. 2006)]. For stimuli with faster FM rates (5 Hz $< f_{FM} <$ 24 Hz), there is an asymmetry between the upper and lower sideband amplitudes: as the modulation frequency increases, the lower sideband level decreases toward the noise floor, whereas the upper sideband level remains well above the noise floor. For the fastest stimuli ($f_{FM} >$ 24 Hz), both upper and lower sidebands decrease to the noise floor. In summary, we observed a two-sideband-to-one-sideband spectral pattern

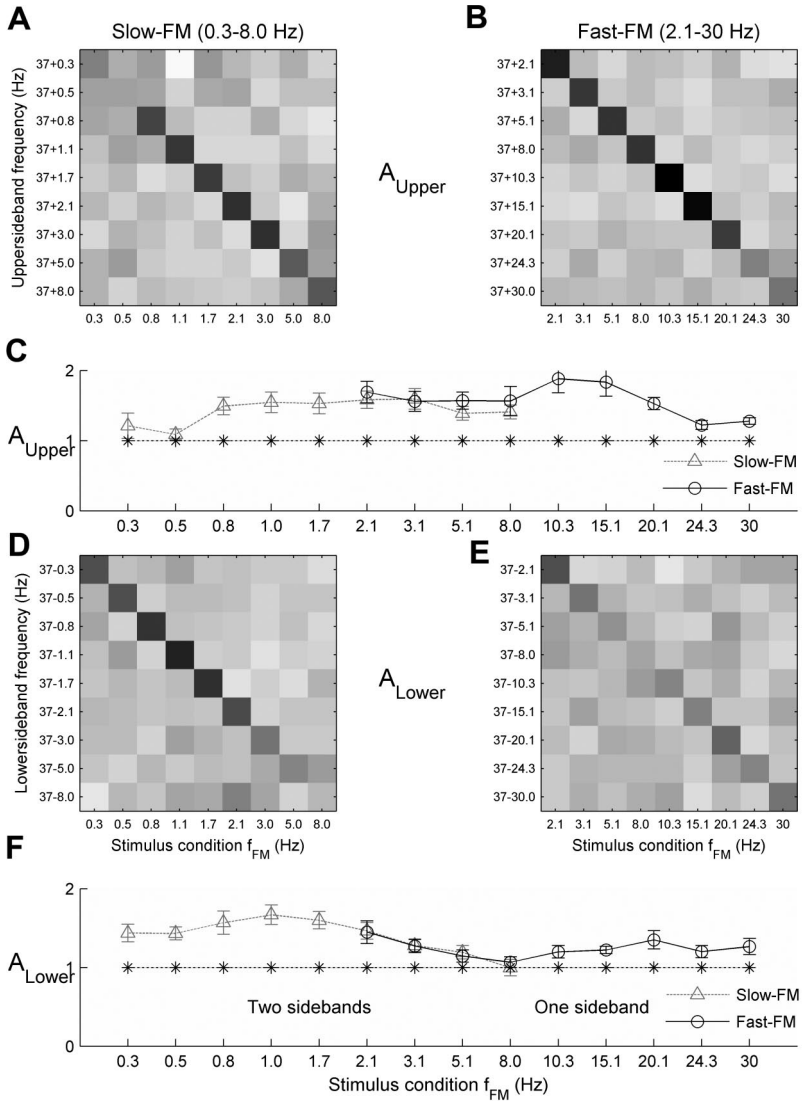

FIG. 3. Amplitude matrix A_{Upper} and A_{Lower} for both the slow-FM experiment (f_{FM}: 0.3–8 Hz) and the fast-FM experiment (f_{FM}: 2.1–30 Hz), and the corresponding diagonal value vectors. *A*: A_{Upper} of the slow-FM experiment. *B*: A_{Upper} of the fast-FM experiment. *D*: A_{Lower} of the slow-FM experiment. *E*: A_{Lower} of the fast-FM experiment. Each box represents the normalized amplitude at the particular target upper sideband frequency (vertical axis) under specific stimulus condition (horizontal axis). *C*: diagonal value vectors of A_{Upper} (gray dotted line: slow-FM experiment; black solid line: fast-FM experiment). *F*: diagonal value vectors of A_{Lower} for both the slow- and fast-FM experiments. The starred lines in the plots indicate the noise floor at each specific target frequency. Note that f_{FM} around 5.0 Hz marked the transition from "2 sidebands" to "1 sideband." All 4 amplitude matrices (*A, B, D,* and *E*) share the same grayscale range: white = 0.7, black = 1.9. Error bars are SE across subjects.

transition with increasing stimulus f_{FM} (≤24.3 Hz) with the transition occurring at f_{FM} ~5 Hz.

Analysis of the $A_{Upperdiff}$ and $A_{Lowerdiff}$ parameters also shows a similar sideband transition occurring at f_{FM} ~5 Hz.

Transition from PM to unreliable encoding-type parameter

Figure 4 summarizes the behavior of the encoding-type parameter α for both the slow FM experiment (gray line) and the fast FM experiment (black line). Figure 4*A* shows the circular mean and SE of α, which lies roughly in the PM encoding region (~π) for slower f_{FM} (<5 Hz) and transitions into a regime of undetermined values with increasing f_{FM} rate

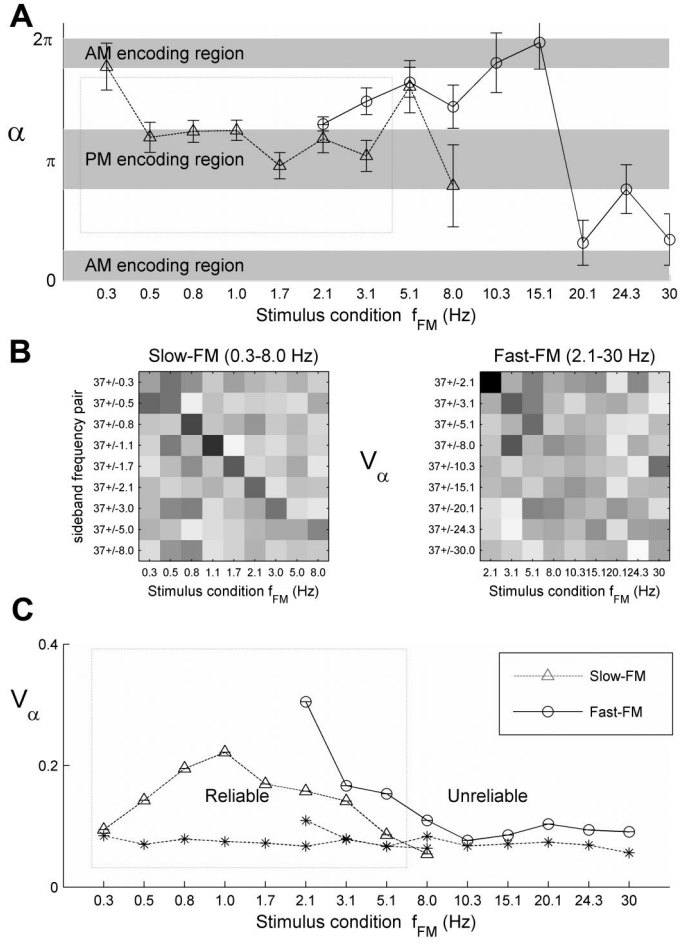

FIG. 4. Encoding-type parameter α and the corresponding vector strength matrix V_α. *A*: α plot for different f_{FM} stimulus conditions (gray dotted line: slow-FM experiment; black solid line: fast-FM experiment) using circular statistics. Gray bars represent the PM encoding region (middle, ~π) and AM region (upper and lower, ~0 or 2π). Error bars are circular SE across all samples. *B*: V_α of both the slow-FM experiment (*left*) and the Fast-FM Experiment (*right*). Each box in the matrix represents the vector strength calculated from all samples (slow-FM experiment: 600 samples; fast-FM experiment: 550 samples), for the specific sideband frequency pair (row) under different stimulus conditions (column). Vector strength is also equal to 1 minus the circular variance of the distribution. The 2 vector strength matrices share the same grayscale range: white = 0.0, black = 0.3. *C*: diagonal vectors of V_α (slow-FM experiment: gray dotted line; fast-FM experiment: black solid line). The starred line indicates the corresponding mean vector strength value of each row representing the background vector strength of α across all 9 stimulus conditions. Note that f_{FM} around 5.0 Hz again marked the transition from "reliable" to "unreliable." The dotted rectangle indicates the reliable range of α, where corresponding v_α is above background level (starred line).

(as stated in the preceding text, the outlier at f_{FM} = 0.3 Hz is due to the narrowband system noise at 37.3 Hz).

V_α, the vector strength of α, was calculated to determine the robustness of this measurement of modulation encoding and the reliability of observed modulation encoding type. Figure 4*B* illustrates the entire matrix V_α and the corresponding diagonal value vectors for both the slow FM experiment and the fast FM experiment. Specifically, the V_α for the slow FM experiment (f_{FM}: 0.3–8 Hz, left matrix of upper panel) manifests a dominantly diagonal pattern, especially for $f_{FM} < 5$ Hz (1st to 7th row), compared with the V_α for the fast FM experiment (f_{FM}: 2.1–30 Hz, right matrix of *top panel*), in which only the first 3 rows (corresponding to f_{FM} of 2.1, 3.1, and 5.1 Hz) show a dominant diagonal. The corresponding diagonal value vectors (*bottom*) decrease to the baseline v_α value as stimulus f_{FM} increases, reflecting that the encoding-type parameter α becomes increasingly noisier and more unreliable for faster stimulus f_{FM} (>5 Hz) with a trend of α shifting to roughly the AM encoding region (~0 or 2π) in Fig. 4*A*. In summary, we observe a transition of α from the PM encoding region (~π) to unreliable and noisy values as the stimulus rate f_{FM} increases, with a transition point of f_{FM} ~5 Hz.

Transition from symmetry to asymmetry in phase

There are two primary motivations to investigate the behavior of $\theta_{Upperdiff}$ and $\theta_{Lowerdiff}$, the two subcomponents of α. First, as stated in the preceding text, we found that α becomes noisier and unreliable for $f_{FM} > 5$ Hz (Fig. 4), but at least the upper sideband response is still significantly elicited (Fig. 3, *A* and *B*), indicating the sustained presence of some form of modulation encoding. Therefore by examining the corresponding changes of these two subcomponents of α, we can demonstrate the underlying reasons for α becoming noisier. Second, we can use these subcomponents to investigate the phase performances for the upper and lower sidebands separately, as we did for amplitude analysis. From the signal processing side, the vector strengths of $\theta_{Upperdiff}$ and $\theta_{Lowerdiff}$ ($v_{Upperdiff}$, $v_{Lowerdiff}$) reflect the temporal precision (latency, starting phase, etc.) of the elicited MEG response.

Figure 5 illustrates the $V_{Upperdiff}$ (*A–C*) and $V_{Lowerdiff}$ (*D–F*) results for both the slow FM experiment (Fig. 5, *A* and *D*) and the fast FM experiment (Fig. 5, *B* and *E*). We can observe the dominantly diagonal pattern in most of the four matrices, indicating that these phase parameters ($\theta_{Upperdiff}$, $\theta_{Lowerdiff}$) manifests smaller variance (larger vector strength) under the corresponding stimulus conditions (compared with other stimulus conditions). In addition, there are clear differences between $V_{Upperdiff}$ (Fig. 5, *A* and *B*) and $V_{Lowerdiff}$ (Fig. 5, *D* and *E*). Specifically, $V_{Upperdiff}$ shows a dominantly diagonal pattern, whereas this pattern is much murkier and noisier in $V_{Lowerdiff}$, especially for the high f_{FM} range (Fig. 5*E*). Such asymmetrical behavior between $V_{Upperdiff}$ and $V_{Lowerdiff}$ is also reflected in Fig. 5, *C* and *F*, which illustrates the corresponding nine-value diagonal value vector of $V_{Upperdiff}$ and $V_{Lowerdiff}$,respectively, for both the slow FM experiment (gray line) and the fast FM experiment (black line). The horizontal starred line indicates the mean vector strength for this phase parameter across all stimulus conditions. Specifically, for stimuli with low f_{FM} (<5 Hz), vector strengths for both $\theta_{Upperdiff}$ and

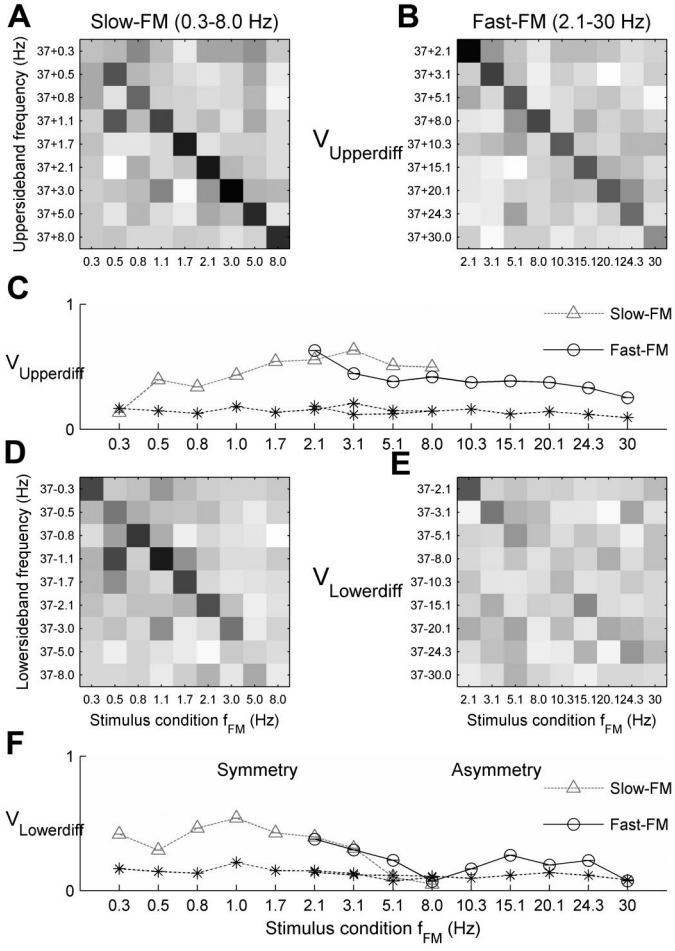

FIG. 5. Phase vector strength matrix $V_{\text{Upperdiff}}$ and $V_{\text{Lowerdiff}}$ for both the slow-FM experiment (f_{FM}: 0.3–8 Hz) and the fast-FM experiment (f_{FM}: 2.1–30 Hz), and the corresponding diagonal value vectors. *A*: $V_{\text{Upperdiff}}$ of the slow-FM experiment. *B*: $V_{\text{Upperdiff}}$ of the fast-FM experiment. *C*: $V_{\text{Lowerdiff}}$ of the slow-FM experiment. *D*: $V_{\text{Lowerdiff}}$ of the fast-FM experiment. Each box represents the calculated vector strength of the specific phase parameter ($\theta_{\text{Upperdiff}}$, $\theta_{\text{Lowerdiff}}$) (vertical axis) under specific stimulus condition (horizontal axis). *C*: diagonal value vectors of $V_{\text{Upperdiff}}$ (gray dotted line: slow-FM experiment; black solid line: fast-FM experiment). *F*: diagonal value vectors of $V_{\text{Lowerdiff}}$ for both the slow-FM experiment and the fast-FM experiment. The starred lines indicate the mean of each corresponding row, indicating the phase vector strength background level. Note that f_{FM} around 5.0 Hz marked the transition from "symmetry" to "asymmetry." All 4 phase vector strength matrices (*A, B, D,* and *E*) share the same grayscale range: white = 0.0, black = 0.65. Error bars are SE across subjects.

$\theta_{\text{Lowerdiff}}$ ($v_{\text{Upperdiff}}$, $v_{\text{Lowerdiff}}$) were significantly above the noise floor (with the exception of the $f_{\text{FM}} = 0.3$ Hz outlier in $v_{\text{Upperdiff}}$, due to system narrowband noise at 37.3). For stimuli with faster FM ($f_{\text{FM}} > 5$ Hz), there is an asymmetry between $v_{\text{Upperdiff}}$ and $v_{\text{Lowerdiff}}$: $v_{\text{Lowerdiff}}$ decreases toward the noise floor (Fig. 5, *A–C*), whereas $v_{\text{Upperdiff}}$ remains well above (*D–F*). In summary, with increases in stimulus f_{FM}, we observe a symmetry-to-asymmetry transition in the vector strength of phase parameters between upper and lower sidebands, where the transition point is $f_{\text{FM}} \sim 5$ Hz. This symmetry-to-asymmetry transition is similar to the two-to-one sideband transition in the amplitude matrix (Fig. 2), indicating a certain relationship between the two groups of parameters: the phase parameters ($V_{\text{Upperdiff}}$, $V_{\text{Lowerdiff}}$) and the amplitude parameters (A_{Upper}, A_{Lower}).

Additionally, $\theta_{\text{Upperdiff}}$ and $\theta_{\text{Lowerdiff}}$ were adjusted to compensate for a 40-ms group delay (latency) estimated by the slope of the $\theta_{\text{Upperdiff}}$-frequency and $\theta_{\text{Lowerdiff}}$-frequency curves. This 40-ms value also matches well with the results of Ross et al. (2000). The circular means and standard errors of the adjusted $\theta_{\text{Upperdiff}}$ and $\theta_{\text{Lowerdiff}}$ are plotted in Fig. 6*A* for comparison with the simulations.

Transition in both amplitude and phase from symmetry to asymmetry

The strong correlation between the phase and amplitude parameters for both the slow FM experiment (triangle) and the fast FM experiment (circle) is summarized in Fig. 6, *C* and *D,* which plots the amplitude asymmetry index AI_{A} and the phase vector strength asymmetry index AI_{V}, respectively, as a function of f_{FM}. Specifically, both AI_{A} and AI_{V} are near zero for the lowest and highest f_{FM} ranges ($f_{\text{FM}} < 5.1$ Hz, $f_{\text{FM}} > 20.1$ Hz), indicating commensurate results in both amplitude and phase reliability between the upper and lower sidebands (as before, the 2 outliers at f_{FM} of 0.3 and 0.5 Hz are due to system narrowband noise at 37.3 and 37.5 Hz). For the middle f_{FM} range (5 Hz $< f_{\text{FM}} <$ 20 Hz), both AI_{A} and AI_{V} increase significantly above zero, indicating the emergence of an asymmetry between the upper and lower sideband responses; here the asymmetry favors the upper sideband in both amplitude and phase. These results are consistent with the previous amplitude, encoding-type parameter, and phase results (Fig. 3–5), and they reconfirm the coding transition from pure PM encoding (2 elicited sidebands, robust phase at both sidebands, α approximately π) to a different encoding strategy (elicited upper sideband only, robust phase at only upper sideband, α becoming noisier and unreliable). In summary, a transition from PM encoding to single sideband encoding (SSB) is confirmed here.

Simulation results

Figure 6 shows simulation results for a single neural population model. The simulation results, a function of both AM index m and phase shift parameter θ are illustrated in Fig. 6, *I–L,* in matrix form. For each θ, all the simulations show complex transitions as m changes. The results for $\theta = \pi/2$ (dotted rectangle in Fig. 6, *I–L*), shown in Fig. 6, *E–H,* show transitions that are similar to those found in the data (Fig. 6, *A–D*), not only for the measured parameters (Fig. 6, *A* and *B*) but also for their distributions (Fig. 6, *C* and *D*). For other values of θ, the matching performance may be good for some of the parameters but not all of them. These results suggest that introduction of fixed 90° phase delay, a quadrature relationship, between the AM contribution to $S(t)$ and the phase modulation contribution to $S(t)$ is necessary to account for the observed PM-to-SSB transition as we observed. This simulation investigates whether a gradual increase in the AM contribution to the response (here by increasing the AM index m in the single neural population model) can account for the observed transition from pure PM response to SSB response. Therefore we compare the simulation performance (Fig. 6, *E–H*) as a function of m with the experiment results (Fig. 6, *A–D*) as a function of stimulus condition f_{FM}. Phase modulation index values other than $\pi/8$ were tested, so no predictions are made regarding this index.

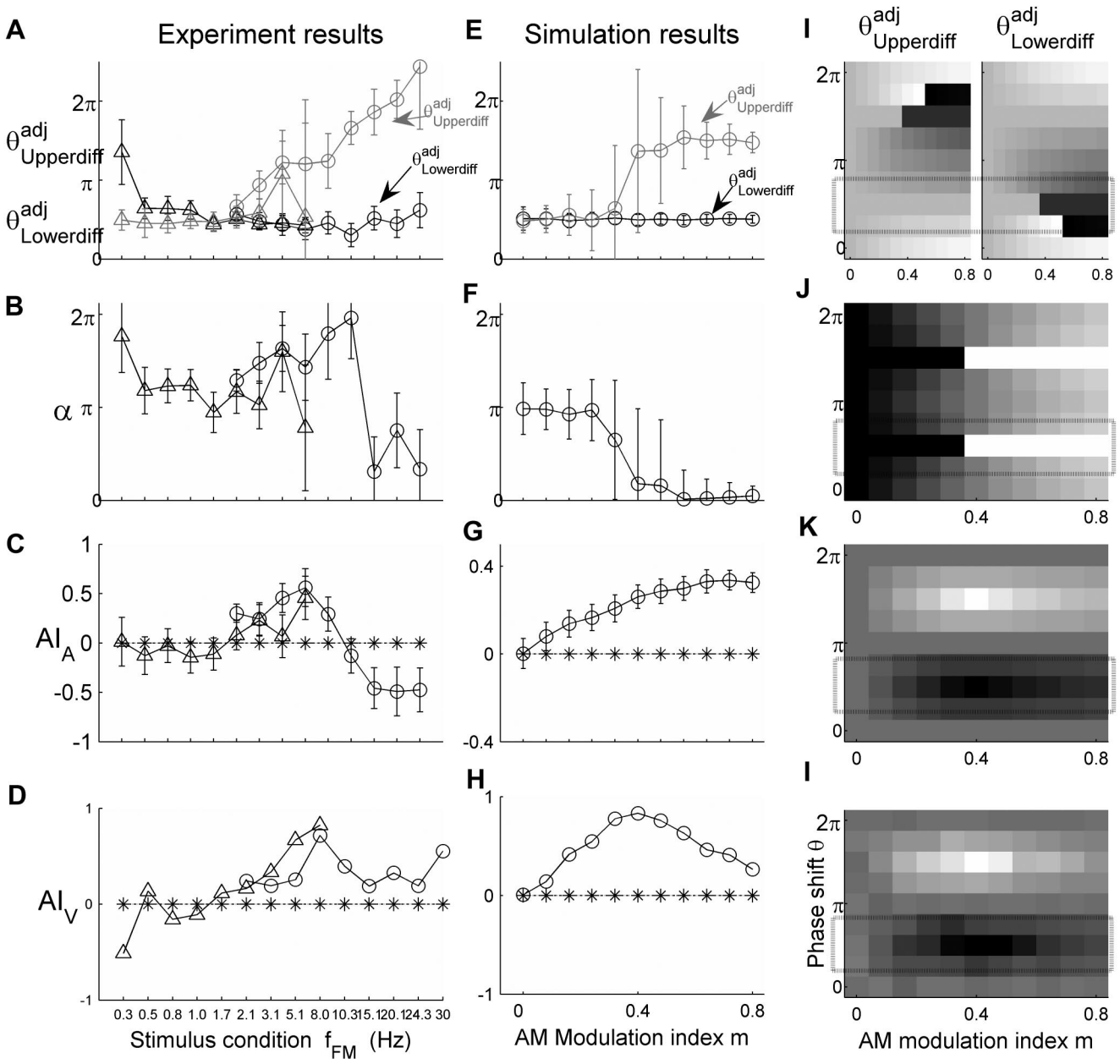

FIG. 6. Comparisons between experiment results (*A–D*, slow-FM experiment: triangle; fast-FM experiment: circle) and simulation results (*I–L*: simulation matrix results as a function of both AM modulation index *m* and phase shift parameter θ; *E–H*: simulation result plots for θ at (π/2). *A, E,* and *I*: $\theta^{adj}_{Upperdiff}$ (black line) and $\theta^{adj}_{Lowerdiff}$ (gray line). *B, F,* and *J*: encoding type parameter α. *C, G,* and *K*: amplitude asymmetry index (AI_A) between upper and lower sideband. *D, H,* and *L*: phase vector strength asymmetry index (AI_V) between phase parameter $\theta^{adj}_{Upperdiff}$ and $\theta^{adj}_{Lowerdiff}$. The starred line at 0 in AI_A and AI_V plots indicate the symmetrical performance between upper and lower sideband performances. Black boxes indicate large values in matrices results. Note that the simulation result plots (*E–H*) reproduce to 1 part of (dotted rectangle) the simulation matrix results (*right*). Note that the simulation for θ at π/2 (*E–H*) matches well with the experimental results (*A–D*): $\theta^{adj}_{Upperdiff}$ (*A* and *E,* black line) remains flat with small error bars; $\theta^{adj}_{Lowerdiff}$ (*A* and *E,* gray line) manifests a rough transition through π with larger error bars; the encoding type parameter α (*B* and *F*) shows a transition from $\sim\pi$ to $\sim$0; both AI_A and AI_V manifest a transition from 0 to positive values (*C, D, G,* and *H*). Error bars are circular SE in *a, b, e,* and *F* and are SE in *C, D, G,* and *H*.

The simulation results for $\theta = [\pi/2$ (Fig. 6, *E–H*) can be divided into three regions: PM-dominated, PM-AM-mixture, and AM-dominated, corresponding to small, middle, and large *m*, respectively. The most interesting and relevant range is the mixture region. Specifically, as the role of the subsidiary AM encoding increases (increasing *m*), $\theta^{adj}_{Upperdiff}$ (black line) remains relatively fixed with small error bars throughout the range of *m*, whereas $\theta^{adj}_{Lowerdiff}$ (gray line) manifests a rough transition through π and with larger error bars. At the same time, the encoding type parameter α shows a transition from PM encoding region ($\sim\pi$) to AM encoding region ($\sim$0). As for the asymmetry index performance, both AI_A and AI_V are strongly positive in the mixture range, reflecting the dominance of the upper sideband in the signals. The simulation results match the empirical results in many facets (Fig. 6, *A–D*), suggesting that the observed transition from a PM encoding signal to a SSB signal may be due to the increasing importance of a subsidiary AM encoding mechanism (invoked in the

simulation by increasing the AM index m) in addition to the already present PM encoding, as a monotonic function of f_{FM}.

Similar simulation results are found from the paired neural population model and thus not illustrated here. Specifically, the simulation results can also be divided into three regions: PM-dominated, PM-AM-mixture, and AM-dominated, corresponding to small, middle, and large τ, respectively. As τ increases, $\theta^{adj}_{Upperdiff}$, $\theta^{adj}_{Lowerdiff}$, α, AI_A, and AI_V of simulated signals showed the similar transition pattern as that of single neural population model in Fig. 6, suggesting that additional involvement of activities of a subsidiary AM encoding neural population in the response of an already present PM encoding neural population could account for the observed transition from pure PM encoding to SSB signal. Importantly, it also requires a 90° phase shift between the two neural populations' modulation signals [$S_{AM}(t)$ and $S_{PM}(t)$]. Such a precise phase relationship between two independent neural populations is an extra required assumption, which leads us to favor and emphasize the single neural population model.

DISCUSSION

In this set of experiments, we have investigated the mechanisms of co-representation of simultaneous acoustic AM and FM, two of the most significant acoustic properties of natural communication sounds. Using sounds with simultaneous sinusoidally modulated amplitude (AM, $f_{AM} = 37$ Hz) and carrier frequencies (FM, $f_{FM} = 0.3$–30 Hz), the elicited MEG responses were analyzed. We observed a transition in the MEG responses, from pure PM encoding signals, to signals containing only the upper sideband in the spectrum (SSB). A neuronal model was constructed and suggested that the introduction of a subsidiary AM encoding mechanism onto the already present PM encoding would explain the occurrence of SSB encoding.

Modulation encoding for feature grouping

Temporal modulation features characterize the dynamics in a sound. AM describes changes in temporal amplitude (envelope), and FM describes changes in carrier frequency (fine structure). Stimuli with temporal modulation features are often used to examine the extent to which sensory neurons can fire spikes following the temporal structures of the stimuli. For this reason, the concept of modulation is useful to describe both the stimulus dynamics and the corresponding stimulus-locked responses. Elhilali et al. (2004) have shown that in ferret AI, neural responses lock not only to envelope dynamics (e.g., AM), but also to the carrier dynamics (e.g., FM). Cariani (2004), among the many possible temporal neural codes, proposes multiplexing, a method widely used in telecommunications, as a perceptual grouping mechanism. With this view, the same neural element may be responsible for both concurrent representation and transmission of multiple signals. In accordance with this proposal, here, by observing a significant spectral peak with robust phase behavior at sideband frequencies, we demonstrate that modulation encoding, an efficient encoding method to multiplex two features' representations, can track independent stimulus AM and FM simultaneously and in a single representation. It provides a natural means of perceptual grouping. This is in contrast to, for instance, the trivial case of responses locking to two simultaneous stimulus modulations only at the two separate rates (e.g., aSSR at the stimulus AM rate and at the stimulus FM rate, with no co-modulation), where the two responses do not fall inside a common, natural grouping.

Neural modulation encoding

The two most simple modulation encoding types are AM encoding and phase modulation (PM) encoding: these arise naturally when the aSSR amplitude or phase depend on the carrier frequency of the stimulus and so would be expected to occur when the carrier frequency is modulated. Correspondingly, neurons employing AM encoding (Luo et al. 2006) and PM encoding (Patel and Balaban 2004) have both been proposed. Both types of neurons fire spikes that are phase-locked to the stimulus AM (at frequency f_{AM}), but they differ in the way they encode FM features. Specifically, from one f_{AM} cycle to the next, the AM encoding neuron changes its firing *rate*, i.e., the magnitude of the envelope of the response over an entire cycle, to represent the stimulus-carrier frequency. In contrast, from one f_{AM} cycle to the next, the PM encoding neuron changes its firing *pattern*, i.e., at which time within the cycle the firing occurs, to represent the stimulus-carrier frequency. In other words, both the AM and PM neurons employ temporal coding to track the AM feature, but, from one f_{AM} cycle to the next, use rate or temporal coding, respectively, to represent the FM feature. Weakly electric fish also provide natural examples of a modulation-encoding neuron. This species needs to compare timing of sensory feedback from electric organ discharges received at different parts of its body surfaces to execute jamming avoidance. Interestingly, amplitude-sensitive and differential phase-sensitive neurons project to an overlapping area where neurons respond to simultaneous amplitude and phase modulations (Heiligenberg and Rose 1986; Kawasaki and Guo 1998).

Coding transitions

We observe a PM-to-SSB transition as f_{FM} increases from 0.3 to 30 Hz. Specifically, stimuli with slow f_{FM} (<5 Hz) elicit both significantly stronger peaks and robust phase at both upper and lower sideband frequencies, and the encoding-type parameter α is robustly within the PM encoding region ($\sim\pi$). As stimulus f_{FM} increases ($5\text{ Hz} < f_{FM} < 20$ Hz), only upper sidebands are elicited and have robust phase, whereas the lower sideband decreases and has noisy phase. Correspondingly, the encoding-type parameter α, the sum of phase parameters for the upper and lower sidebands, also becomes noisy and unreliable. We propose the engagement of a subsidiary AM encoding in addition to the already present PM encoding, which combine in such a way as to cancel the lower sideband, and thus accounts for the observed PM-to-SSB transition. Specifically, for stimuli with slow f_{FM}, the neurons rely solely on a PM encoding mechanism to track the AM and FM features simultaneously. As stimulus f_{FM} increases, these neurons also begin to employ an AM encoding mechanism, also co-representing AM and FM features. Then both AM and PM encoding mechanisms are present, adding constructively (for the upper sideband) and destructively (for the lower sideband) to generate a SSB signal and used for concurrent encoding.

The observed transition >5 Hz serves an additional role as a sanity check. If the observed modulation response produced

only a single type of modulation (e.g., only PM or only AM) over a wide range of rates, it is quite possible that the observed modulation responses might merely be an epiphenomenon, having nothing to do with neural coding per se. The observed transition, however, especially to such a novel modulation response mechanism (SSB), makes this scenario substantially less plausible.

It is apparent that a PM encoding mechanism, as seen for slow f_{FM} stimuli, requires more temporal precision and resolution for co-representation and is thus also more resource intensive than an AM encoding mechanism, since it changes the spike firing time to indicate the carrier frequency. AM encoding, in contrast, requires less temporal precision and resolution and only roughly needs to change firing rate to track FM. Therefore it is reasonable that only PM encoding is involved when tracking stimuli with slower carrier frequency dynamics and that for tracking stimuli with faster FM requiring more neural resources, the relative contribution of the coarser and more economic AM encoding mechanism is increasingly engaged. These findings parallel findings in marmoset (Lu et al. 2001), using click train stimuli, where there is a temporal-to-rate coding switch as the click trains became faster. The different transitions frequencies (5 Hz found here vs. their ~30 Hz) are undoubtedly due to the different stimuli (click trains vs. concurrent AM-FM stimuli) and their different encodings (straight rate/temporal vs. modulation encoding). Our results are also consistent with fMRI experiments (Giraud et al. 2000; Harms and Melcher 2002) that have documented changes in the shape and magnitude of sustained responses to AM and FM stimuli as modulation frequency increases. Psychophysical studies have also proposed FM-to-AM transduction (Saberi and Hafter 1995) and two-stage detection (Moore and Sek 1996) for FM sound perception. Although this body of research refers to pure AM or FM detection, the underlying ideas apply straightforwardly to our hypothesis.

Addressing alternative explanations

An alternative explanation for the asymmetry between upper and lower sideband performance that must be ruled out is the different signal-to-noise ratios at those frequencies. For example, the decreased performance at the lower sidebands for faster stimuli might be due to the stronger background noise at lower frequencies, where the lower sideband frequency ($f_{AM} - f_{FM}$) for higher f_{FM} is located, which in turn would lead to asymmetric results. To test this explanation, we analyzed the direct FM aSSR (aSSR at f_{FM}, not at a sideband), using the same amplitude matrix analysis as that of the sideband frequencies. Because some of the target f_{FM} frequencies (0.3–30 Hz) are located in an overlapping frequency region to that for lower sideband frequencies with deteriorated performance, if the poor performance for those lower sidebands was due to noisier background, the background noise would also influence the performance of the aSSR at f_{FM}. However, we did not find any decreased performance at this region; on the contrary, the responses at those f_{FM} frequencies were strongly elicited. Therefore the very same analysis on the same frequency region but using different criteria leads to diverse results, supporting that it is an encoding transition rather than a change in signal-to-noise that accounts for the asymmetry between upper and lower sideband performances. Additionally, the sideband amplitude analyses did not strongly depend on which sideband amplitude parameter pairs were used, A_{Lower} versus A_{Upper} (which depend strongly on the signal to noise), or $A_{Lowerdiff}$ versus $A_{Upperdiff}$ (which depend only weakly on the signal to noise).

Another possibility that can be ruled out is that it might not be a transition per se but rather an epiphenomenon due to a phase modulation index that grows with f_{FM}. An increasing phase modulation index (i.e., the parameter set to $\pi/8$ in the simulations) might be thought to mimic the loss of sideband amplitude because it would spread the response power across more distant frequencies. The is can be ruled out for two reasons: first, only the parameter $A_{Lowerdiff}$ vanishes at the transition, not $A_{Upperdiff}$, whereas an increase in the phase modulation index would cause both to vanish or even if there were a coincidental increase in power, neither would vanish; and second, as stated in Luo et al. (2006), increasing the phase modulation index does not affect the encoding-type parameter α until it becomes quite large ($\sim 3\pi$), and so the amplitude reduction and change in encoding-type parameter a would not co-occur simultaneously.

It can also be shown that the transition is not present in the auditory nerve and so must be generation centrally (e.g. cortically). Simulations of auditory nerve fibers of varying characteristic frequency, responding to our stimuli with varying f_{AM}, were undertaken using gammatone filterbanks from the auditory toolbox (Slaney 1998). These simulations show that in the auditory nerve's response to the our stimuli show only AM and not PM encoding: there is an overall AM at f_{AM} (the neural carrier) and the amplitude of that modulation is itself modulated at f_{FM}. There is no evidence for PM encoding or a transition from AM encoding to any other modulation encoding, in the auditory nerve. Furthermore the AM encoding observed in this auditory nerve model is not seen at all in our cortical data. This effectively rules out any peripheral-only explanation of the modulation encoding transition seen in cortex.

Neurons performing specific phase delay

In our neuronal model, AM encoding signals required a specific phase relationship (90° phase shift) with PM encoding signals; this accounts well for the observed SSB signals. Neurons with a specific phase shift relative to other neurons have been observed in several studies. For example, in a sound localization study by Fitzpatrick et al. (2000), three types of ITD-sensitive neurons in the inferior colliculus (IC) were found (peak, trough, and intermediate); these differ in their characteristic phase even when they have the same characteristic delay. In other words, their response patterns are phase-shifted versions of one another. In an ITD discrimination model study, Hancock and Delgutte (2004) have also proposed that the involvement of a phase shift mechanism in a system of solely internal delays could predict psychophysical performances more accurately. In the visual domain, "lagged cells" have been reported in both LGN and V1 (DeValois et al. 2000; Saul and Humphrey 1990; Saul et al. 2005). These cells show a specific lagged phase (e.g., by 90°) in their responses compared with ordinary "nonlagged cells" and are argued to solve the problem of encoding long and variable delays because a given phase difference provides longer time differences at low

frequencies. Thus the hypothesized phase shift in our model is not unrealistic, and most importantly, constructing an additional phase-shifted version of the encoding signal using a different coding scheme (here AM modulation encoding) seems to be an efficient way to establish a new way of representing modulation features.

Relationship with general neural oscillations

Brain rhythms are widely studied and are argued to have important functions in the cerebral cortex (see review by Sejnowski and Paulsen 2006). It has been suggested that gamma-band oscillations (~40 Hz) may solve the binding problem (Bertrand and Tallon-Baudry 2000; Llinas and Ribary 1993; Singer and Gray 1995) by synchronously referring diverse fragmented sensory feature representations into a coherent temporal framework to achieve a single cognitive state. This 40-Hz oscillatory activity has been proposed to result from the resonant properties of the thalamocortical system (Llinas 2000) and interactions between excitatory and inhibitory neurons (Freeman 2000). It has also been suggested that the elicited aSSRs reflect the resetting of this 40-Hz brain rhythm by transients in the sensory input, which could also explain the maximum aSSR for modulation frequency ~40 Hz across various stimulus types (Picton et al. 1987; Rees et al. 1986; Regan 1989; Ross et al. 2000; Stapells et al. 1984). A study of the aSSR to pure AM sound (Ross et al. 2000) systematically examined the effects of stimulus properties (modulation frequency, carrier frequency) on the aSSR (amplitude and phase). Their results suggest that properties of the 40-Hz brain oscillation are modulated by the incoming sensory stimulus. Therefore an alternative explanation for the encoding transition from the perspective of systems neuroscience is that it reflects a transition between brain states. Specifically, for stimuli with slow dynamics, the brain's 40-Hz rhythms are set by changes in the amplitude of the stimulus envelope (at rate f_{AM}), and the timing of this resetting response, which is reflected in the starting phase of this signal, depends on the fine structure of the incoming stimulus, here, the carrier frequency. As the stimulus fine structure modulations become faster, there arises a more complex pattern in the brain oscillations, which are still reset by envelope changes, whereas both the resetting gain and resetting phase depend on the incoming stimulus carrier frequency.

MEG and studies of neural coding

The majority of work on neural coding is principally based on data from single-unit recordings. Furthermore, computational models concerning coding are almost exclusively based on such data. The work presented here illustrates that there can be very explicit linking hypotheses that bridge the gap between animal and human work. Hemodynamic data (coming from fMRI or PET recordings) also provide valuable data in this regard but are only indirect indices of neural activity because their time scales are limited to the order of seconds. In contrast, the electrophysiological MEG data described in this work show that reasonable assumptions about neural coding, coupled with computational analyses, can tie together work across vastly separated scales. Our data suggest that there is a population of cortical neurons (or a paired set of populations) that co-encode independent AM and FM stimulus modulations in a naturally grouped manner. These neurons have not been recorded from individually in this experiment, yet their electromagnetic signature is evident via the MEG signal.

ACKNOWLEDGMENTS

We are grateful to J. Walker for excellent technical assistance and S. Hoffman for extensive proofreading.

GRANTS

This research was supported by National Institute of Deafness and Other Communications Disorders Grant R01 DC-05660 to D. Poeppel and Chinese Academy of Science 973 Program Grant 2005CB522800.

REFERENCES

Ahissar E, Nagarajan S, Ahissar M, Protopapas A, Mahncke H, Merzenich MM. Speech comprehension is correlated with temporal response patterns recorded from auditory cortex. *Proc Natl Acad Sci USA* 98: 13367–13372, 2001.

Bertrand O, Tallon-Baudry C. Oscillatory gamma activity in humans: a possible role for object representation. *Int J Psychophysiol* 38: 211–223, 2000.

Boemio A, Fromm S, Braun A, Poeppel D. Hierarchical and asymmetric temporal sensitivity in human auditory cortices. *Nat Neurosci* 8: 389–395, 2005.

Cariani PA. Temporal codes and computations for sensory representation and scene analysis. *IEEE Trans Neural Netw* 15: 1100–1111, 2004.

De Valois RL, Cottaris NP, Mahon LE, Elfar SD, Wilson JA. Spatial and temporal receptive fields of geniculate and cortical cells and directional selectivity. *Vision Res* 40: 3685–3702, 2000.

deCharms RC, Blake DT, Merzenich MM. Optimizing sound features for cortical neurons. *Science* 280: 1439–1443, 1998.

Depireux DA, Simon JZ, Klein DJ, Shamma SA. Spectro-temporal response field characterization with dynamic ripples in ferret primary auditory cortex. *J Neurophysiol* 85: 1220–1234, 2001.

Dimitrijevic A, John MS, van Roon P, Picton TW. Human auditory steady-state responses to tones independently modulated in both frequency and amplitude. *Ear Hear* 22: 100–111, 2001.

Drullman R, Festen JM, Plomp R. Effect of temporal envelope smearing on speech reception. *J Acoust Soc Am* 95: 1053–1064, 1994.

Efron B, Tibshirani RJ. *An Introduction to the Bootstrap.* London: Chapman and Hall/CRC, 1994.

Eggermont JJ. Temporal modulation transfer functions for AM and FM stimuli in cat auditory cortex. Effects of carrier type, modulating waveform and intensity. *Hear Res* 74: 51–66, 1994.

Eggermont JJ, Ponton CW. The neurophysiology of auditory perception: from single units to evoked potentials. *Audiol Neurootol* 7: 71–99, 2002.

Elhilali M, Fritz JB, Klein DJ, Simon JZ, Shamma SA. Dynamics of precise spike timing in primary auditory cortex. *J Neurosci* 24: 1159–1172, 2004.

Fisher NI. *Statistical Analysis of Circular Data.* Cambridge, UK: Cambridge, 1996.

Fitzpatrick DC, Kuwada S, Batra R. Neural sensitivity to interaural time differences: beyond the Jeffress model. *J Neurosci* 20: 1605–1615, 2000.

Freeman WJ. *How brains make up their minds.* New York: Columbia University Press, 2000.

Gaese BH, Ostwald J. Temporal coding of amplitude and frequency modulation in the rat auditory cortex. *Eur J Neurosci* 7: 438–450, 1995.

Giraud AL, Lorenzi C, Ashburner J, Wable J, Johnsrude I, Frackowiak R, Kleinschmidt A. Representation of the temporal envelope of sounds in the human brain. *J Neurophysiol* 84: 1588–1598, 2000.

Haller S, Radue EW, Erb M, Grodd W, Kircher T. Overt sentence production in event-related fMRI. *Neuropsychologia* 43: 807–814, 2005.

Hancock KE, Delgutte B. A physiologically based model of interaural time difference discrimination. *J Neurosci* 24: 7110–7117, 2004.

Harms MP, Melcher JR. Sound repetition rate in the human auditory pathway: representations in the waveshape and amplitude of fMRI activation. *J Neurophysiol* 88: 1433–1450, 2002.

Hart HC, Hall DA, Palmer AR. The sound-level-dependent growth in the extent of fMRI activation in Heschl's gyrus is different for low- and high-frequency tones. *Hear Res* 179: 104–112, 2003.

Heil P. Auditory cortical onset responses revisited. I. First-spike timing. *J Neurophysiol* 77: 2616–2641, 1997.

Heiligenberg W, Rose G. Gating of sensory information: joint computations of phase and amplitude data in the midbrain of the electric fish, *Eigenmannia. J Comp Physiol* 159: 311–324, 1986.

John MS, Picton TW. Human auditory steady-state responses to amplitude-modulated tones: phase and latency measurements. *Hear Res* 141: 57–79, 2000.

Kawasaki M, Guo YX. Parallel projection of amplitude and phase information from the hindbrain to the midbrain of the African electric fish *Gymnarchus niloticus*. *J Neurosci* 18: 7599–7611, 1998.

Klein DJ, Konig P, Kording KP. Sparse spectrotemporal coding of sounds. *Eurasip J Appl Sig P* 2003: 659–667, 2003.

Kowalski N, Depireux DA, Shamma SA. Analysis of dynamic spectra in ferret primary auditory cortex. I. Characteristics of single-unit responses to moving ripple spectra. *J Neurophysiol* 76: 3503–3523, 1996.

Langers DRM, Backes WH, van Dijk P. Spectro-temporal features of the auditory cortex: the activation in response to dynamic ripples. *Neuroimage* 20: 265–75, 2003.

Lewicki MS. Efficient coding of natural sounds. *Nat Neurosci* 5: 356–363, 2002.

Liang L, Lu T, Wang X. Neural representations of sinusoidal amplitude and frequency modulations in the primary auditory cortex of awake primates. *J Neurophysiol* 87: 2237–2261, 2002.

Liegeois-Chauvel C, Lorenzi C, Trebuchon A, Regis J, Chauvel P. Temporal envelope processing in the human left and right auditory cortices. *Cereb Cortex* 14: 731–740, 2004.

Llinas R. *I of the Vortex: From Neurons to Self.* Cambridge, MA: MIT Press, 2000.

Llinas R, Ribary U. Coherent 40-Hz oscillation characterizes dream state in humans. *Proc Natl Acad Sci USA* 90: 2078–2081, 1993.

Lu T, Liang L, Wang X. Temporal and rate representations of time-varying signals in the auditory cortex of awake primates. *Nat Neurosci* 4: 1131–1138, 2001.

Luo H, Wang Y, Poeppel D, Simon JZ. Concurrent encoding of frequency and amplitude modulation in human auditory cortex: MEG evidence. *J Neurophysiol* 96: 2712–2723, 2006.

Lutkenhoner B, Steinstrater O. High-precision neuromagnetic study of the functional organization of the human auditory cortex. *Audiol Neurootol* 3: 191–213, 1998.

Miller LM, Escabi MA, Read HL, Schreiner CE. Spectrotemporal receptive fields in the lemniscal auditory thalamus and cortex. *J Neurophysiol* 87: 516–527, 2002.

Moore BC, Sek A. Detection of frequency modulation at low modulation rates: evidence for a mechanism based on phase locking. *J Acoust Soc Am* 100: 2320–2331, 1996.

Nicolelis MAL, Ghazanfar AA, Faggin BM, Votaw S, Oliveira LMO. Reconstructing the engram: simultaneous, multisite, many single neuron recordings. *Neuron* 18: 529–537, 1997.

Oertel D. Encoding of timing in the brain stem auditory nuclei of vertebrates. *Neuron* 19: 959–962, 1997.

Oertel D. The role of timing in the brain stem auditory nuclei of vertebrates. *Annu Rev Physiol* 61: 497–519, 1999.

Oppenheim AV, Willsky AS. *Signals and Systems.* Englewood Cliffs, NJ: Prentice-Hall, 1997.

Papoulis A. *The Fourier Integral and its Applications.* New York: McGraw-Hill, 1962.

Patel AD, Balaban E. Temporal patterns of human cortical activity reflect tone sequence structure. *Nature* 404: 80–84, 2000.

Patel AD, Balaban E. Human auditory cortical dynamics during perception of long acoustic sequences: phase tracking of carrier frequency by the auditory steady-state response. *Cereb Cortex* 14: 35–46, 2004.

Phillips DP, Hall SE, Boehnke SE. Central auditory onset responses, and temporal asymmetries in auditory perception. *Hear Res* 167: 192–205, 2002.

Picton TW, John MS, Dimitrijevic A, Purcell D. Human auditory steady-state responses. *Int J Audiol* 42: 177–219, 2003.

Picton TW, Skinner CR, Champagne SC, Kellett AJ, Maiste AC. Potentials evoked by the sinusoidal modulation of the amplitude or frequency of a tone. *J Acoust Soc Am* 82: 165–178, 1987.

Rees A, Green GG, Kay RH. Steady-state evoked responses to sinusoidally amplitude-modulated sounds recorded in man. *Hear Res* 23: 123–133, 1986.

Regan D. *Human Brain Electrophysiology: Evoked Potentials and Evoked Magnetic Fields in Science and Medicine.* New York: Elsevier, 1989.

Rose HJ, Metherate R. Auditory thalamocortical transmission is reliable and temporally precise. *J Neurophysiol* 94: 2019–2030, 2005.

Ross B, Borgmann C, Draganova R, Roberts LE, Pantev C. A high-precision magnetoencephalographic study of human auditory steady-state responses to amplitude-modulated tones. *J Acoust Soc Am* 108: 679–691, 2000.

Ross B, Herdman AT, Pantev C. Stimulus induced desynchronization of human auditory 40-Hz steady-state responses. *J Neurophysiol* 94: 4082–4093, 2005.

Saberi K, Hafter ER. A common neural code for frequency- and amplitude-modulated sounds. *Nature* 374: 537–539, 1995.

Saul AB, Carras PL, Humphrey AL. Temporal properties of inputs to direction-selective neurons in monkey V1. *J Neurophysiol* 94: 282–294, 2005.

Saul AB, Humphrey AL. Spatial and temporal response properties of lagged and nonlagged cells in cat lateral geniculate nucleus. *J Neurophysiol* 64: 206–224, 1990.

Schreiner CE, Urbas JV. Representation of amplitude modulation in the auditory cortex of the cat. I. The anterior auditory field (AAF). *Hear Res* 21: 227–241, 1986.

Schreiner CE, Urbas JV. Representation of amplitude modulation in the auditory cortex of the cat. II. Comparison between cortical fields. *Hear Res* 32: 49–63, 1988.

Sejnowski TJ, Paulsen O. Network oscillations: emerging computational principles. *J Neurosci* 26: 1673–1676, 2006.

Shannon RV, Zeng FG, Kamath V, Wygonski J, Ekelid M. Speech recognition with primarily temporal cues. *Science* 270: 303–304, 1995.

Simon JZ, Wang Y. Fully complex magnetoencephalography. *J Neurosci Methods* 149: 64–73, 2005.

Singer W, Gray CM. Visual feature integration and the temporal correlation hypothesis. *Annu Rev Neurosci* 18: 555–586, 1995.

Slaney M. *Auditory Toolbox.* Technical Report 1998-010, Interval Research, <http://rvl4.ecn.purdue.edu/~malcolm/interval/1998-010/>, 1998.

Smith EC, Lewicki MS. Efficient auditory coding. *Nature* 439: 978–982, 2006.

Smith ZM, Delgutte B, Oxenham AJ. Chimaeric sounds reveal dichotomies in auditory perception. *Nature* 416: 87–90, 2002.

Stapells DR, Linden D, Suffield JB, Hamel G, Picton TW. Human auditory steady state potentials. *Ear Hear* 5: 105–113, 1984.

Viemeister NF. Temporal modulation transfer functions based upon modulation thresholds. *J Acoust Soc Am* 66: 1364–1380, 1979.

Wang XQ, Lu T, Liang L. Cortical processing of temporal modulations. *Speech Commun* 41: 107–121, 2003.

Wilson MA, McNaughton BL. Dynamics of the hippocampal ensemble code for space. *Science* 261: 1055–1058, 1993.

Zatorre RJ, Belin P, Penhune VB. Structure and function of auditory cortex: music and speech. *Trends Cogn Sci* 6: 37–46, 2002.

Zeng FG, Nie K, Stickney GS, Kong YY, Vongphoe M, Bhargave A, Wei C, Cao K. Speech recognition with amplitude and frequency modulations. *Proc Natl Acad Sci USA* 102: 2293–2298, 2005.

Zwicker E. Die Grenzen der Horbarkeit der Amplitudenmodulation und der Frequenzmodulation eines Tones. *Acustica* 2: 125–133, 1952.